Fluvial landscape development in the southwestern Kalahari during the Holocene - Chronology and provenance of fluvial deposits in the Molopo Canyon

Ramisch, Arne; Bens, Oliver; Buylaert, Jan-Pieter; Eden, Marie; Heine, Klaus; Hürkamp, Kerstin; Schwindt, Daniel; Völkel, Jörg

Published in:
Geomorphology

Link to article, DOI:
10.1016/j.geomorph.2016.12.021

Publication date:
2017

Document Version
Peer reviewed version

Fluvial landscape development in the southwestern Kalahari during the Holocene – chronology and provenance of fluvial deposits in the Molopo Canyon

Authors: Arne Ramisch[1*], Oliver Bens[2], Jan-Pieter Buylaert[3,4], Marie Eden[1], Klaus Heine[5], Kerstin Hürkamp[6], Daniel Schwindt[1] and Jörg Völkel[1]

Affiliations:

1 Technical University of Munich, Centre of Life Sciences Weihenstephan, Hans-Carl-von-Carlowitz-Platz 2, 85354 Freising, Germany

2 GFZ German Research Centre for Geoscience, Telegrafenberg, 14473 Potsdam, Germany

3 Nordic Laboratory for Luminescence Dating, Department of Geosciences, University of Aarhus, Risø Campus, Denmark

4 Center for Nuclear Technologies, Technical University of Denmark, Risø Campus, Denmark

5 University of Regensburg, 95053 Regensburg, Germany

6 Helmholtz Zentrum München, German Research Center for Environmental Health, Ingolstädter Landstraße 1, 85764 Neuherberg, Germany

***Corresponding author, present address:** GFZ German Research Centre for Geoscience, Telegrafenberg, 14473 Potsdam, Germany. E-Mail: arne.ramisch@gfz-potsdam.de

Keywords: Holocene; Southwestern Kalahari; Fluvial Morphodynamics

Highlights:

- ➔ First quasi-continuous record of fluvial morphodynamics during the Holocene in the southwestern Kalahari
- ➔ Evidence for a changing influence of circulation systems on flash flood regimes in the southern African interior
- ➔ Indication of limited sediment supply from the southwestern Kalahari to the Orange River

Abstract

The Southern Kalahari Drainage network is in a key position to analyze spatiotemporal changes in the tropical easterly and the temperate westerly circulation over the Southern African subcontinent. However, due to the prevailing aridity, paleoenvironmental archives within the southwestern Kalahari are sparse and often discontinuous. Hence, little is known about Holocene environmental change in this region. This study focuses on reconstructing paleoenvironmental change from the timing and provenance of fluvial deposits located within the Molopo Canyon, which connects the Southern Kalahari Drainage to the perennial flow regime of the Orange River. To gain insight into temporal aspects of fluvial morphodynamics within the Molopo Canyon, the entire variety of fluvial landforms consisting mainly of slope sediments, alluvial fans and alluvial fills were dated using Optically Stimulated Luminescence (OSL). We additionally applied a provenance analysis on alluvial fill deposits to estimate potential sediment source areas. Source areas were identified by analyzing the elemental and mineralogical composition of tributaries and eolian deposits throughout the course of the lower Molopo. The results allow the first general classification of fluvial landscape development into three temporally distinct deposition phases in the southern Kalahari: (1) A phase of canyon aggradation associated with short lived and spatially restricted flash floods during the early to mid-Holocene; (2) A phase of fan aggradation indicating a decrease in flood intensities during the mid- to late Holocene; (3) A phase of canyon aggradation caused by the occurrence of supra-regional flood events during the Little Ice Age. We interpret the observed spatiotemporal deposition patterns to latitudinal shifts of the tropical easterly circulation in the early to mid-Holocene and the temperate westerly circulation in the late Holocene. However, despite marked changes in the provenance and timing of fluvial deposits in the Molopo Canyon throughout the Holocene, our analysis did not detect a contribution of sediments originating from the Kalahari interior to the deposition of alluvial fills. These results suggest that the Southern Kalahari drainage remained endorheic and therefore disconnected from the Orange River throughout the Holocene.

1. Introduction

Environmental change over southern Africa is driven by the interaction of major atmospheric and oceanic circulation systems of the southern hemisphere. The ocean-atmosphere interaction leads to the establishment of two rainfall regimes over continental settings of southern Africa (after Chase and Meadows, 2007): (a) A summer rainfall regime driven by the poleward displacement of the ITCZ convection belt during austral summer and (b) a winter rainfall regime driven by the equatorward displacement of frontal systems in austral winter. The landward advection of oceanic moisture for both regimes is connected to the tropical easterly (for a) and temperate westerly (for b) circulations, which results in a spatial differentiation of southern Africa in a summer rainfall zone (SRZ) in the east and a winter rainfall zone (WRZ) in the west of the subcontinent (Fig. 1a). Both zones are separated by a zone influenced by both regimes, called the year round rainfall zone (YRZ). Rainfall intensities in both rainfall regimes are projected to decrease in response to a projected rise in global temperatures (Christensen et al., 2013). Due to the overlap of the WRZ and SRZ circulation over the southwestern Kalahari, the study of Holocene environmental change inferred from sedimentary archives in this region offers insight into the environmental response to climate variations and may shed light on future climate dynamics under changing climatic conditions.

The prevailing South African climate regimes were subject to temporal and spatial variability during the Holocene as evidenced by paleoenvironmental archives on the subcontinent (e.g., Chase and Meadows, 2007; Chase et al., 2009, 2010, 2011, 2012, 2015a, b) and adjacent oceans (e.g., Hahn et al., 2015; Zhao et al., 2016). The long-term moisture evolution in the SRZ and WRZ during the Holocene shows an anti-phase relationship (Tyson, 1986; Cockroft, 1987; Hahn et al., 2015; Zhao et al., 2016) with temporally distinct optima within each zone. The anti-cyclical patterns in moisture evolution are generally ascribed to latitudinal shifts in the easterly and westerly circulation in response to orbital and oceanic forcings (Hahn et al., 2015). The southwestern Kalahari is in a key region to assess the impact of such spatiotemporal shifts in circulation systems on the hydroclimate of the southern African interior, resulting from its location close to present-day borders of the climate regimes (Fig. 1a). However, archives of Holocene hydrological changes in this region are scarce due to prevailing arid conditions and generally constrained by a predominance of eolian landforms (e.g., Dougill and Thomas, 2001; Bateman et al., 2003; Stone and Thomas, 2008), hiatuses in continuous archives such as speleothems (Brook et al., 2010) or major fluvial sedimentation phases prior to the Holocene (Heine, 1990; Hürkamp et al., 2011). Moisture in this arid to semi-arid environment is predominantly supplied episodically during rain events of high magnitude. Due to a relatively

sparse vegetation cover, high stream powers during flood events can cause extensive erosion and deposition along ephemeral channel reaches, making the fluvial landscape susceptible to climatic change. Hence, in the absence of continuous archives, a reliable source of paleoenvironmental change are fluvial deposits (Mann and Meltzer, 2007). Surprisingly, besides scarce evidence for fluvial activity phases within the lower Molopo area (Heine, 1990; Shaw et al., 1992; Nash, 1996; Hürkamp et al., 2011), little is known about fluvial dynamics in the southwestern Kalahari during the Holocene.

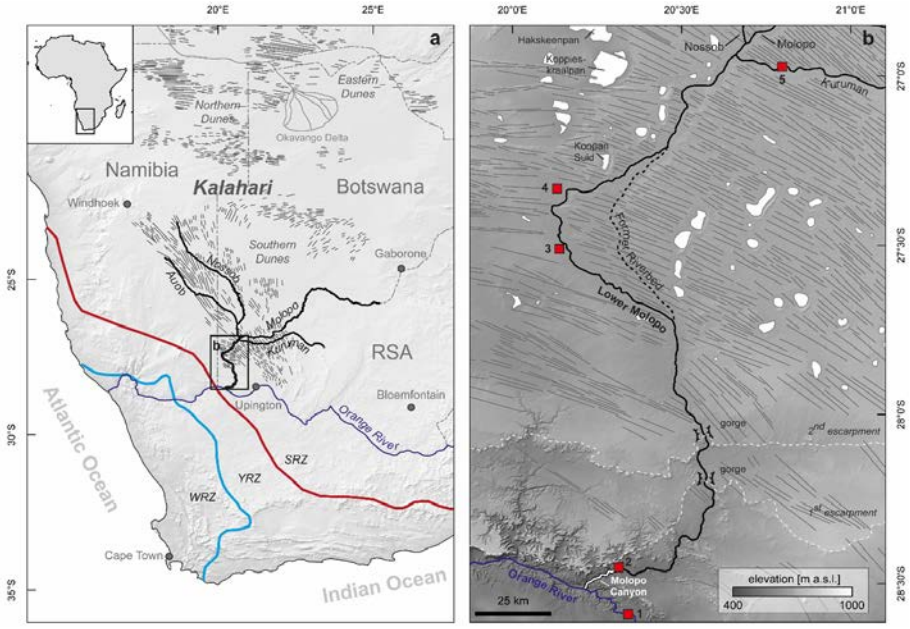

Fig. 1: The southern Kalahari Drainage network in southern Africa. (**a**) Regional overview of the Southern Kalahari and the endorheic southern Kalahari drainage network. Boundaries of present-day rainfall regimes (after Chase and Meadows, 2007) are depicted as a red line for the summer rainfall zone (SRZ) and as a blue line for the winter rainfall zone (WRZ). Both zones are spatially separated by the year round rainfall zone (YRZ). The spatial distribution of major dune fields within the Kalahari are redrawn and named after Thomas et al. (2000). (**b**) Topographical overview of the lower Molopo and its embedding landscape. Grey lines depict idealized dune orientation. Landmarks are depicted as red rectangles: 1 - Upington; 2 – Riemvasmaak; 3 – Noenieput; 4 – Abiquas Puts; 5 - Askham

The present study aims to identify spatiotemporal changes in fluvial dynamics in the southwestern Kalahari during the Holocene by reconstructing fluvial landscape development in the Molopo Canyon. The canyon is situated at the mouth of the presently dry lower Molopo

104 which connects the ~250,000 km² large area of the exorheic Southern Kalahari Drainage
105 (termed after Thomas and Shaw, 1991) to the perennial flow regime of the Orange River (Fig.
106 1b). Considering a potential scarcity and infrequency of fluvial deposits within this arid
107 environment, we base our reconstruction on the entire variety of fluvial landforms which mainly
108 consist of slope sediments, alluvial fans and alluvial fills. To identify major phases of fluvial
109 activity during the Holocene, we establish a chronology for fluvial deposits in the Molopo
110 Canyon using quartz OSL-dating. To gain insight into spatial sediment dynamics during phases
111 of increased fluvial activity, we apply a provenance analysis on fluvial sediments stored in
112 alluvial fill sequences. Furthermore, potential environmental causes of the observed
113 spatiotemporal shifts in fluvial sediment dynamics during the Holocene within the lower
114 Molopo will be discussed in a supra-regional framework.

2. Study Area

The lower Molopo (20.1-20.6°E and 20.7-28.5°S) drains the ephemeral flow regimes of the Aoub, Nossob, Molopo and Kuruman rivers (called Southern Kalahari Drainage network, Fig. 1a) into the perennial flow regime of the Orange River. The lower Molopo exhibits a gentle stream gradient with an altitudinal change of ~400 m in its entire flow length of ~250 km, corresponding to an average flow gradient of <0.2%. The climatic conditions are characterized by a true desert BWh climate (Köppen climate classification) with an annual precipitation of ~180 mm and a temperature of 20.4°C as recorded at the climate station Upington (Fig. 1b) during the period of 1951 to 1990. The southwestern Kalahari is therefore the only true desert environment of the otherwise semi-arid to sub-humid Kalahari (Hürkamp et al., 2011).

The topography of the lower Molopo landscape is characterized by an approximately latitudinal alignment of two escarpments (further denoted as 1st and 2nd escarpment from south to north, Fig. 1b), resulting in a step like configuration of the landscape. In particular, the latitudinal course of the 2nd escarpments at ~28.1°S (Fig. 1b) delineates a major topographical boundary and divides the lower Molopo into an eolian and a fluvial landscape. The eolian landscape north of the 2nd escarpment is characterized by the gently inclined Kalahari Plateau. The entire Plateau is covered by longitudinal dune complexes belonging to the southern dune field (Fig. 1a). Recent to sub-recent fluvial morphodynamics are only evident in between the Molopo – Kuruman confluence and Koopan Suid (Fig. 1b) where dune complexes only partly traverse the river bed of the lower Molopo, suggesting fluvial sediment input of the Kuruman River during episodically occurring flood events (Heine, 1981). Between Koopan Suid and the 2nd escarpment, the entire river bed is covered by dune complexes with only isolated geomorphic signs of recent to sub-recent fluvial morphodynamics. The fluvial landscape south of the 2nd escarpment is characterized by numerous tributaries and their associated catchments which originate in their western reaches from the 1st and 2nd escarpments. Bedrock geology consists of metamorphic rocks belonging to the Neoproterozoic Nama Group in the north and the Mesoproterozoic Namaqua-Natal Belt (Garzanti et al., 2014). South of Riemvasmaak (28.45°S), the lower Molopo enters a ~500 m wide and ~100 m deep canyon dominated by metamorphic rocks of the Nama group. The river bed of the lower Molopo Canyon is covered by sediments of fluvial origin, which mainly consist of alluvial fills and alluvial fans from local tributaries.

3. Material and Methods

Fluvial landforms in the lower Molopo Canyon were identified and investigated during two field campaigns in 2010 and 2013. The investigation was conducted throughout the course of the canyon. The suite of fluvial landforms consists mainly of slope deposits, alluvial fans and fluvial terraces. Based on field observations, we chose three major study sections within the canyon (Fig. 2b) which contain the previously identified fluvial landforms. We generated geomorphological sketches based on field observations and satellite imagery of each section (Fig. 2b) and conducted eight sediment profiles in representative landforms (Fig. 2). Grain size and soil colour of sediments were estimated in the field. Three key profiles in alluvial fills were identified and each observed layer sampled for provenance analysis.

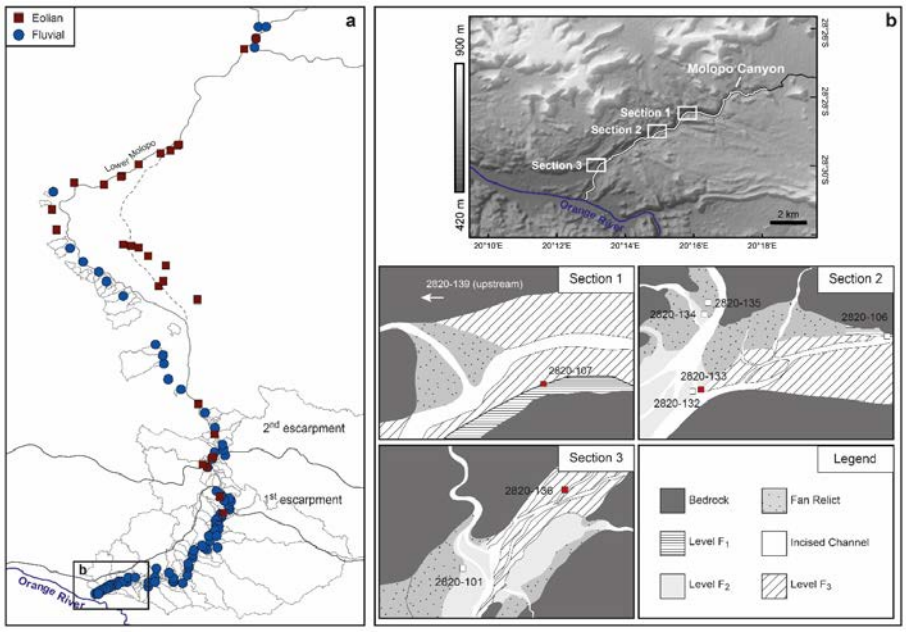

Fig. 2: Sample locations and research sections throughout the lower Molopo. (**a**) Sample location of reference samples (eolian – OA; fluvial – OF). Grey polygons correspond to tributary catchments. (**b**) Location (top) and geomorphological sketches (bottom) of research sections within the Molopo Canyon. Profile locations are illustrated as white rectangles, key profiles are illustrated as red rectangles with the corresponding profile number.

3.1 Luminescence dating

Fifteen samples for OSL dating were collected from representative fluvial deposits; samples were taken at the top and base of each profile. The light-proof sample tubes were opened under

subdued orange light at the Nordic Laboratory for Luminescence dating (Aarhus University, DTU Risø Campus, Denmark). The outer light-exposed part of the sediment was first used to determine the field and saturation water content and then air dried, ground, heated at 450°C for 24 h and cast in wax before being counted on a laboratory gamma spectrometer following the procedures described in Murray et al. (1987). The resulting radionuclide concentrations were converted to dry dose rates using the conversion factors published by Guérin et al. (2011). The inner material was wet-sieved to the 180-250 µm fraction (samples 145423 and -28, 90-300 µm), treated with 10% HCl, 10% H_2O_2 and etched in 10% HF for 40 min. K-feldspar rich extracts were separated from quartz using a heavy liquid (LST "Fastfloat", 2.58 g/ml) density separation. Finally, the quartz extract was treated with 40% HF for 60 min and subsequently washed in 10% HCl for 1 h. The fractions were washed with distilled water between each step. After drying, quartz grains were mounted as large (8 mm) multigrain aliquots on stainless steel discs and K-rich feldspar as small (2 mm) aliquots on stainless steel cups. Luminescence measurements were made using standard Risø TL/OSL DA-20 readers (Thomsen et al., 2006). Luminescence from quartz was detected through a Hoya U-340 glass filter (centred on 340 nm, FWHM = 80 nm) and luminescence from feldspar through a combination of Schott BG-3 and BG-39 filters (centred on 390 nm, FWHM=100 nm). The quartz purity was confirmed by the absence of a significant infra-red stimulated luminescence (IRSL) signal. Quartz was stimulated at 125°C for 40 s using blue LEDs and net OSL signals were calculated using early background subtraction to maximize the contribution of the fast component (Cunningham and Wallinga, 2010). The first 0.8 s of the signal minus a background from the following 0.8 s was chosen for signal and background integration, respectively. Quartz equivalent doses were measured using a SAR (Murray and Wintle, 2000, 2003) protocol using a preheat of 200°C for 10 s and a cut-heat to 160°C. At the end of each SAR cycle the aliquots were stimulated with blue light at 280°C to reduce recuperation. Feldspar aliquots were measured using a post-IR IRSL protocol suitable for young samples based on Madsen et al. (2011). Aliquots were preheated to 180°C for 60 s followed by 200 s IR stimulation at 50°C (IR50 signal) and 150°C (pIRIR150 signal). A high temperature IR clean-out at 200°C was inserted after each SAR cycle. The first 2 s of the decay curve minus a background from the last 20 s was used for feldspar dose calculations.

3.2 Provenance analysis: mineralogy, geochemistry and statistics

To identify major sediment provinces throughout the course of the lower Molopo, we sampled potential sediment sources from 93 tributaries (denoted as OF-sample) and 32 eolian deposits (denoted as OA-sample) throughout the course of the lower Molopo (Fig. 2a) during a field

campaign in 2015. Fluvial reference samples (OF) were taken near their mouth from the uppermost 10 cm of deposits which showed evidence for recent fluvial deposition. All samples were sieved after drying to a grain size <2 mm prior to the elemental and mineralogical analysis. No additional grain size differentiation was imposed on the bulk fine fraction in order to avoid a potential grain-size bias due to mineral enrichment or depletion within single grain size fractions as a result of hydrological sorting effects during entrainment-deposition cycles as described by Garzanti et al. (2009). Subsequently, samples were powdered prior to further analysis.

X-ray diffractometry (XRD) was applied to estimate the mineralogical composition and the relative abundance of single minerals in all sediment samples. Dry and milled bulk sediment samples were analyzed by XRD using a Siemens (Germany) D5000 X-ray diffractometer (40 kV, 40 mA, from 2 to 85°, step-rate 0.05°, Co k-alpha radiation). Mineral concentrations were calculated semi-quantitatively from main peak area intensities (measured in counts per second) of mineral phases after base-line and quartz peak correction. Relative concentrations were calculated by the ratio between main peak intensities of a given mineral phase and the total intensity of main peaks of all identified mineral phases. The identification of mineral phases from XRD patterns was verified by petrographic microscopy of samples containing representative amounts of a respective mineral phase.

To estimate the elemental composition of sediment samples we applied an X-ray fluorescence (XRF) analysis to the dry and milled bulk sediment samples. To save time and capacities given the number of sediment samples (n=185), we used a portable NITON XL 722s spectrometer to estimate element concentrations from powdered samples (for details, see Raab et al., 2005). To validate the elemental composition measured with the portable XRF device, we additionally estimated element concentrations quantitatively for 21 samples (13 reference samples and 11 profile samples) with a Panalytical Axios Advanced wavelength-dispersive spectrometer. Powdered samples were melted into lithium tetaborate disks using FLUXANA FX-X65 prior to analysis.

The statistical provenance analysis was applied using a Fuzzy C-Means algorithm (FCM) (Dunn, 1973; Bzedek, 1981) on the previously estimated mineralogical and elemental composition of reference samples, following the approach recently established by Opitz et al. (2016) and Ramisch et al. (2016) for lacustrine sediments on the Tibetan Plateau. FCM partitions a given data set iteratively into a number of prescribed cluster centers based on an objective function and assigns each sample with a membership degree (μ) to a respective cluster center. Membership degrees are in a theoretical range of 0 for absent membership and 1 for

231 complete membership. Prior to the clustering routine, we applied a range transformation as
232 described in Milligan and Cooper (1988) to the raw data set. Subsequently, the FCM clustering
233 routine was carried out on reference samples (OF- and OA-samples) in 10^4 iterations to avoid
234 spurious local minima in the objective function using a fuzzyfier of 2.0. To validate a suitable
235 cluster number, we calculated the Xie-Beni index (XBi) (Xie and Beni, 1991; Wu and Yang,
236 2005) for each cluster partition in a range between two to nine cluster centers. The XBi
237 measures the separation between the cluster center and the inner cluster compactness in terms
238 of µ. An optimal cluster number is indicated by a minimum of the XBi. After applying the FCM
239 routine to the reference data set, we estimated similarities of alluvial fill sediments to the
240 previously estimated cluster center using a fuzzy assignment function presented in Opitz et al.
241 (2016) and Ramisch et al. (2016) with a fuzzyfier of 2.0.

4. Results

4.1 Luminescence chronology

Table S1 summarises the radionuclide concentrations and calculated dry gamma and beta dose rates. Assumed life-time average water contents and resulting total dose rates to sand-sized quartz and K-feldspar grains are given in Table 1. Water contents are based on the assumption that the sediments remained very well-drained for the majority of the burial life-time in this desert environment. They are consistent with assumed water contents previously used for OSL dating in the southern Kalahari (Hürkamp et al., 2011). Radionuclide activities in these sediments are high resulting in quartz total dose rates ranging from ~4.6 to ~7.5 Gy/ka. A representative quartz SAR OSL dose response curve is shown in Fig S1a. The quartz OSL signals are dominated by a fast component (inset Fig. S1a) and the overall dose recovery ratio is satisfactory for this material (0.93 ± 0.02, $n = 45$) suggesting that we can accurately measure a quartz dose given in the laboratory prior to any heat treatment. Feldspar IR_{50} and $pIRIR_{150}$ dose recovery ratios are also satisfactory as indicated by the slopes close to unity in the measured to given dose plots (Fig. S2). Quartz OSL, IR_{50} and $pIRIR_{150}$ equivalent doses and ages are summarized in Table 1.

A potential problem in dating alluvial and slope sediments is the incomplete resetting of the luminescence signal at deposition (e.g., Rittenour, 2008). Murray et al. (2012) proposed that one can check for completeness of quartz bleaching by comparing quartz OSL results with those obtained using less-bleachable IRSL signals. This approach has now been used by a significant number of studies (e.g., Guérin et al., 2015; Reimann et al., 2015; Sugisaki et al., 2015; Long et al., 2015; Peeters et al., 2016; Rémillard et al., 2016) for a range of IR and pIRIR stimulation temperatures and sedimentary environments. Fig. S3 shows the $pIRIR_{150}$ ages as a function of the quartz OSL ages. Here we consider samples to be well-bleached (open symbols) when the $pIRIR_{150}$ ages agree with the quartz ages at one standard deviation (4 samples denoted with "confident" in Table 1). Comparison of the IR_{50} ages with the quartz OSL ages indicates that a additional two samples can be identified as probably well-bleached for quartz (grey symbols in Fig. S4). For the remaining samples we cannot be confident about the completeness of quartz bleaching. However, it should be noted that for most of these samples (145421,-22,-23,-26,-27,-28) the quartz ages are very young (few hundred years) which puts an upper limit of a few tens (to hundreds) of years to the potential degree of incomplete bleaching of quartz. In the following section the quartz OSL ages are used for interpretation.

Table 1. Summary of quartz and feldspar luminescence data. Equivalent dose (D_e), number of aliquots contributing to D_e, total dose rates, assumed water content (10% of saturation), quartz OSL and uncorrected feldspar IR_{50} and $pIRIR_{150}$ ages. The completeness of quartz bleaching at deposition is checked by comparing quartz ages with $pIRIR_{150}$ and IR_{50} ages based on Murray et al. (2012).

Site and sample code	Lab code	Landform	Depth (cm)	Quartz D_e (Gy)	Qz. n	Feldspar IR_{50} D_e (Gy)	Feldspar $pIRIR_{150}$ D_e (Gy)	Feldsp. n	Quartz dose rate (Gy ka^{-1})	Feldspar dose rate (Gy ka^{-1})	w.c. (%)	Quartz age (ka)	IR_{50} age (ka)	$pIRIR_{150}$ age (ka)	Quartz well-bleached?
2820-139 KAL 66	145429	Slope Sediments	40	127 ± 8	27	208±4	399±18	6	5.12 ± 0.24	6.04±0.24	4	25 ± 2	34±2	66±4	Not confident
2820-139 KAL 67	145430	Slope Sediments	60	56.7 ± 3.7	30	135±9	287±21	6	4.95 ± 0.23	5.80±0.23	4	11.5 ± 0.9	23±2	50±4	Not confident
2820-101 KAL 23	145415	Alluvial Fan	35	9.5 ± 0.7	23	10.2±0.9	16.5±2.1	15	6.43 ± 0.30	7.29±0.31	3	1.47 ± 0.13	1.40±0.14	2.3±0.3	Probably
2820-101 KAL 24	145416	Alluvial Fan	300	36.9 ± 3.1	24	34±2	61±5	15	5.69 ± 0.27	6.55±0.27	4	6.48 ± 0.63	5.2±0.3	9.3±0.8	Probably
2820-134 KAL 59	145424	Alluvial Fan	20	37.0 ± 1.8	25	27.4±1.7	41±4	12	6.57 ± 0.32	7.48±0.32	3	5.6 ± 0.4	3.7±0.3	5.5±0.6	Confident
2820-135 KAL 60	145425	Alluvial Fan	40	19.8 ± 0.9	25	15.7±1.8	25±3	21	7.50 ± 0.37	8.35±0.37	2	2.6 ± 0.2	1.9±0.2	3.0±0.4	Confident
2820-106 KAL 27	145417	Alluvial Fill	30	33.8 ± 1.4	27	21.9±1.2	30.1±1.7	12	5.49 ± 0.27	6.38±0.27	2	6.17 ± 0.42	3.4±0.2	4.7±0.3	Confident
2820-106 KAL 28	145418	Alluvial Fill	100	40.4 ± 1.6	27	n.a.	n.a.	n.a..	4.55 ± 0.21	n.a.	4	8.88 ± 0.58	n.a.	n.a.	n.a.
2820-107 KAL 29	145419	Alluvial Fill	30	42.2 ± 2.1	26	23.3±1.9	35±2	12	6.92 ± 0.34	7.80±0.34	2	6.10 ± 0.44	3.0±0.3	4.5±0.3	Confident
2820-132 KAL 57	145422	Alluvial Fill	30	3.96 ± 0.24	36	12.0±3.0	20±5	20	7.26 ± 0.35	7.51±0.31	3	0.64 ± 0.05	1.6±0.4	2.7±0.7	Not confident
2820-132 KAL 56	145421	Alluvial Fill	70	2.14 ± 0.19	26	15.7±2.3	32±6	23	6.19 ± 0.29	7.92±0.34	3	0.29 ± 0.03	2.0±0.3	4.1±0.7	Not confident
2820-133 KAL 58	145423	Alluvial Fill	70	2.41 ± 0.30	32	17.4±5.0	25±7	19	6.14 ± 0.31	6.98±0.31	2	0.39 ± 0.05	2.5±0.7	3.6±1.1	Not confident
2820-136 KAL 61	145426	Alluvial Fill	40	0.79 ± 0.07	31	n.a.	n.a.	n.a.	4.91 ± 0.24	n.a.	2	0.16 ± 0.02	n.a.	n.a.	n.a.
2820-136 KAL 62	145427	Alluvial Fill	65	1.54 ± 0.11	30	5.2±1.0	8.2±1.3	24	4.89 ± 0.24	5.79±0.24	2	0.32 ± 0.03	0.90±0.18	1.42±0.23	Not confident
2820-136 KAL 63	145428	Alluvial Fill	135	3.08 ± 0.23	30	10±4	13±4	14	6.09 ± 0.29	6.90±0.30	3	0.51 ± 0.05	1.45±0.58	1.9±0.6	Not confident

Notes: Quartz and feldspar grain size was 180-250 µm except for samples 145423 and 145428 for which it was 90-300 µm. Feldspar data is not available (n.a.) for two samples due to unsuccessful K-rich feldspar extraction. Feldspar dose rate contains an internal dose rate component from beta decay of internal ^{40}K assuming a K content of 12.5±0.5% K (Huntley and Baril, 1997). Total dose rates contain a contribution from the cosmic ray dose rate taking into account latitude/longitude of the site and sample burial depth following Prescott and Hutton (1994).

4.2 Litho- and chronostratigraphy of sedimentary archives

Fig. 3 illustrates the temporal distribution of estimated ages during the last ~12 ka differentiated by the type of archive. All archives are described in terms of their geomorphological setting, lithostratigraphy as well as chronology in the following sub-sections.

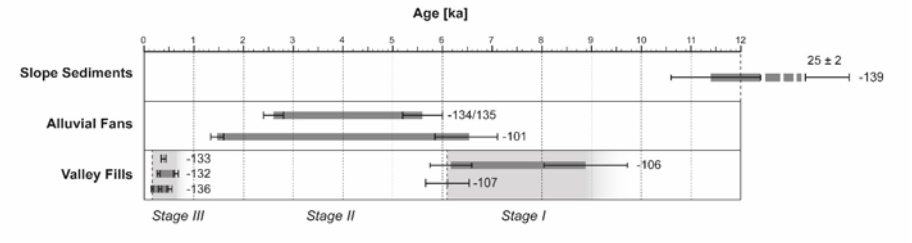

Fig. 3: OSL-dating results for sedimentary archives within the lower Molopo Canyon. Each sedimentary profile is depicted as a grey block and associated with the corresponding profile number (for spatial reference, see Fig. 2). Black lines delineate the 2 sigma range for dating results of the top and base of each profile.

Slopes

Profile 2820-139 is located in the middle section of the canyon on slopes created by the incision of a tributary feeding the lower Molopo with an associated drainage area of 5 km². Slopes at this location are steeply inclined with an angle of ~20°. The profile (605 m a.s.l.) is situated ~110 m above the recent Molopo channel bed. It consists of very poorly sorted, angular clasts without discernable bedding, ranging from fine sand to boulders of ~3 m in diameter. Luminescence ages of samples KAL 66 and 67, taken from lenses of fine sediments within the profile, suggest a deposition between the Last Glacial Maximum and the early Holocene between 25 ± 2 and 11.5 ± 0.9 ka. However, it should be noted that these ages may overestimate the true timing of deposition due to an incomplete bleaching of the quartz grains in this section (Table 1, Fig. S3).

Alluvial Fans

Two alluvial fans situated within the reaches of the canyon were analyzed in terms of their lithostratigraphy and chronology. The first fan is located in study section 2 (Fig. 2) at the confluence of two bedrock channels originating from the 1st escarpment with the Molopo channel bed. At this location, the Molopo Canyon is ~320 m wide. The fan is located at the northern side of the canyon and associated with a cumulative drainage area of ~50 km² from both tributaries. The fan is heavily dissected by the present channels of the tributaries originating from the north as well as the Molopo channel bed in the south, leading to an

arrangement of several inactive relict fans. Profiles 2820-134 and-135 were conducted at the base and top of the northernmost relict fan in between the recent channel beds of the two tributaries, mainly for age estimation purposes. The sediments consist of poorly sorted, sub-angular sediments with a mode in the coarse sand fraction, ranging from fine sand to boulders of ~50 cm without discernible bedding. Age estimates for the deposition of the fan range from at least 5.6 ± 0.4 ka at the base (sample KAL 59 in profile -134) to 2.6 ± 0.2 ka at the top (profile -135) of the relict fan. Both samples KAL59 and 60 are confidently expected to be well-bleached (Table 1, Fig. S3)

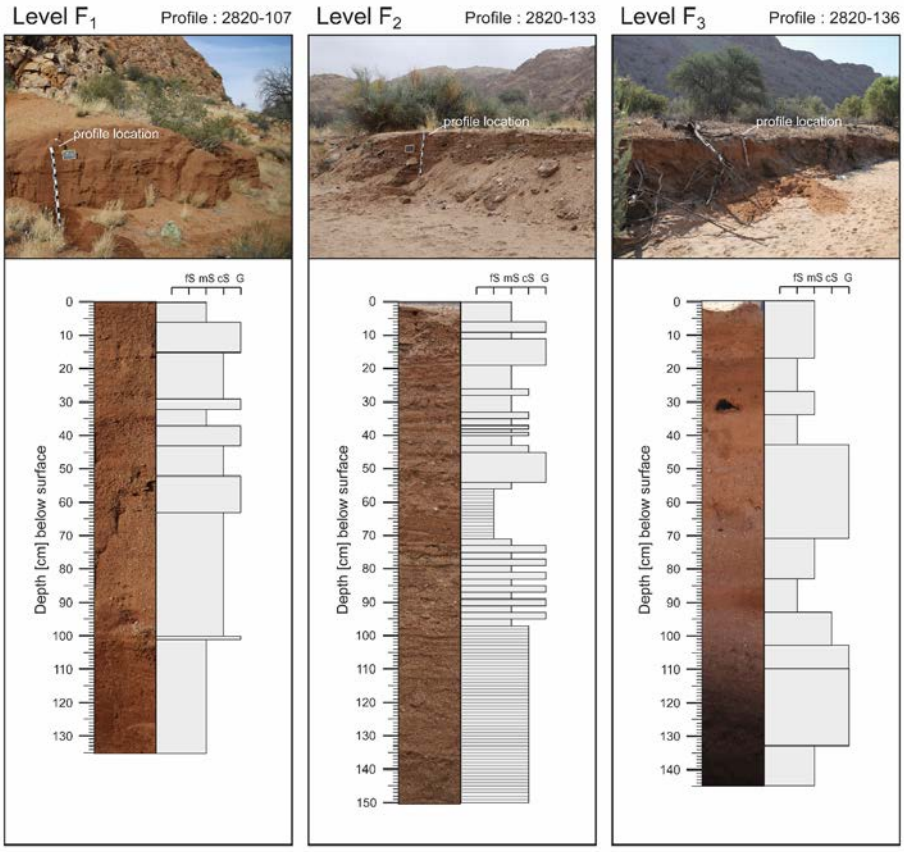

Fig. 4: Lithostratigraphical sketches of sedimentary profiles in three alluvial fill levels (F_1 to F_3) of the lower Molopo Canyon. Layering and dominant grain sizes of each profile are illustrated as grey rectangles. Each profile is accompanied by a photo of the depositional surroundings at the top of the figure.

The second fan is located in the lower reaches of the canyon in study section 3 (Fig. 2), ~1.6 km upstream of the Molopo-Orange confluence in a ~500 m wide section of the canyon. The fan is strongly dissected by the recent channel bed of its associated tributary (~10 km² drainage area) as well as the recent Molopo channel bed. At the profile location 2820-101, the fan reaches a height of ~2.5 m above the channel bed. The sediments of the profile mainly consist of reddish brown, unsorted sands with a mode in the coarse sand fraction. A varying content of angular gravel between 10% and 90% is the main discrimination between different layers in the otherwise unstratified bedding. The quartz OSL ages range from 6.48 ± 0.63 ka (sample KAL24, 300 cm depth) at the base of the profile to 1.47 ± 0.13 ka at the top (sample KAL23, 30 cm depth). The quartz OSL signals of these sediments were probably well-bleached at deposition (Table 1, Fig. S4). The ages are also in stratigraphic order.

Valley fills

Valley fills are deposited throughout the course of the lower Molopo Canyon. Fills occur in three distinct vertical levels, labelled according to their relative height above the present Molopo channel bed from F_1 (highest) to F_3 (lowest).

Level F_1 (~4 m above present Molopo channel bed): Deposits of level F_1 are only preserved in extreme lateral slip-off slopes of the canyon in study sections 2 and 3 (Fig. 2). Sediments of this level mainly consist of reddish-brown, poorly sorted, coarse sand. Profile 2820-107 in section 1 (Fig. 4) shows a sub-horizontal bedding with individual layers ranging from 3 to 37 cm in thickness. Individual layers consist of matrix supported, greyish, sub-angular and partly aligned gravel up to a diameter of 5 cm, deposited without grading structures. All studied deposits of level F_1 are covered by slope debris, likely resulting from its lateral position near the canyon walls. Age estimations suggest deposition of fill level F_1 ranging from 8.88 ± 0.58 ka (sample KAL28) at the base of profile 2820-106 to 6.17 ± 0.42 ka (sample KAL27) at the top of profile 2820-106 and 6.10 ± 0.44 ka (KAL29) at the top of profile 2820-107. Samples KAL 27 and 29 are well-bleached based on a comparison with feldspar (Table 1, Fig. S3). For KAL28 we have no feldspar data, but given that this sample is taken in a similar deposit it is likely that also this sample was well-bleached at deposition and the quartz OSL age is thus probably reliable.

Level F_2 (~1.5 m above present Molopo channel bed): Deposits of level F_2 are located in between relict alluvial fans and the recent Molopo channel bed in study sections 1 and 2 (Fig. 2). The morphological setting suggests deposition within a prograding fan environment associated with the erosion of relict fans upstream. Sediments of level F_2 in section 2 consist of interbedded layer types (1 and 2), which mainly differ in their colour and mean grain size. Layer

type 1 consists of reddish brown, well sorted, fine to medium sand while layer type 2 consists of bright greyish, poorly sorted, coarse sand to gravel. The vertical alternation of both layer types as observed in profile 2820-133 is illustrated in Fig. 4. The layer thickness of both layer types increase towards the top of the profile from a mean thickness of ~1 cm between a depth of 150 and 56 cm to around 5 cm in the upper 56 cm of the profile. Besides the characteristic paragenesis of both layer types, sub-angular clasts up to a diameter of 30 cm occur throughout the lateral extension of profile 2820-133. Dating results of profile 2820-132 show an inverted age-depth relation, with ages ranging from 0.64 ± 0.05 ka at 30 cm depth (KAL57) to 0.29 ± 0.03 ka at 70 cm depth (KAL56). However, the OSL age sampled at the top of the neighboring profile 2820-133 of 0.39 ± 0.05 ka confirms a genesis of F_2 during the latter half of the last millennium. We cannot exclude partial bleaching of quartz for these three samples. Hence the ages may overestimate the true age of deposition by a few decades to hundreds of years (see section 4.1).

Level F_3 (~1.2 m above present Molopo channel bed): Deposits of level F_3 are located throughout the present Molopo channel bed as observed in all sections. The deposits are dissected by a network of anastomosing channels formed by the Molopo, generating several longitudinal bars composed of deposits of F_3. Sediments of F_3 as preserved in profile 2820-136 (Fig. 4) consist of thick bedded layers ranging from 7 to 26 cm. Layers mainly differ in their colour and grain size with bright greyish, poorly sorted sands accompanied by sub-angular gravel up to 2 cm in diameter dominating the lower parts of the profile (145 to 43 cm depth), and reddish brown, sorted, fine to medium sands dominating the top (43 to 0 cm depth) of the profile. Three OSL ages (taken in profile 2820-136) suggest a similar depositional age to sediments of level F_2, ranging from at least 0.51 ± 0.05 to 0.16 ± 0.02 ka. The fact that these young ages are in stratigraphic order supports the hypothesis that partial bleaching of quartz is not a significant problem.

4.3 Mineralogy and geochemistry

We identified 13 mineral phases from X-ray diffraction patterns of bulk sediments collected from alluvial sediments (in three profiles of level F_3 to F_1) as well as tributary (OF) and eolian sediments (OA) throughout the course of the lower Molopo. The mineral spectrum is dominated by the appearance of silicates, with the tectosilicates quartz, K-feldspar and plagioclase present in all analyzed samples with a cumulated mean of 97.5%. In addition to four other silicate phases (almandine, illite, hornblende and mica), we detected evaporates (halite), carbonates (dolomite and calcite) and iron oxides (magnetite) in at least 50 samples. The appearance of

single mineral phases as verified by petrographic microscopy was observed above an approximate diffraction threshold of ~50 cps of its respective main diffraction peak.

4.4 Statistical Provenance Analysis

To identify major sediment provinces within the reaches of the lower Molopo, we applied a FCM cluster algorithm on the mineralogical and elemental composition of reference samples collected from fluvial sediments of tributaries and eolian deposits. We selected single provenance markers for the clustering routine from the set of identified mineral phases and elements. The selection was based on theoretical considerations as well as empirical observations concerning the reliability of the provenance signal of each marker. We excluded all mineral phases from the analysis, which are potentially affected by early-diagenesis as, for example, due to post-burial precipitation (i.e., calcite, dolomite and halite). Further, we excluded hematite (detected in only five reference samples) from the analysis considering its potential depletion downstream and the resulting limitations for detection in fluvial sediments. For geochemical markers, we only included elements in the cluster analysis which were (a) detected by both XRF measurements and (b) show a very high correlation ($r>0.95$, corresponding to >90% explained variance) between element concentrations estimated by both XRF methods.

A cluster number of three was chosen based on a minimum in XBi of 0.1940 as computed from 10^4 simulations. The mineralogical and elemental composition of cluster center 1 to 3 is presented in Fig. 5. Cluster 1 is mainly characterized by high concentrations of the phyllosilicates, plagioclase, and K-feldspar, and low quartz concentrations resulting in a low Qz/Fsp ratio. Additionally, cluster 1 reveals the highest concentrations of hornblende, magnetite, illite and mica compared to the other clusters. The geochemical fingerprint of cluster 1 is dominated by high concentrations of Rb, Zn, K and Zr. Cluster 2 is characterized by intermediate concentrations of most mineral phases in comparison to mineral concentrations in clusters 1 and 2. The major distinction between cluster 2 and the other clusters is a high concentration of almandine as well as high concentrations of the elements Fe, Mn and Ti. Cluster 3 is poor in all analyzed minerals and elements with the exception of quartz, resulting in a high Qz/Fsp ratio. The distribution of membership degrees (μ) of reference samples to clusters 1, 2 and 3 shows a distinct spatial pattern (Fig. 6). This pattern allows a classification of the lower Molopo into three main sediment source areas. The first source area (cluster 1) consists of tributaries supplying the lower reaches of the lower Molopo in close vicinity to the Orange-Molopo confluence. Tributaries of the Molopo Canyon dominate this source area (Fig.

6a). The second source area (cluster 2) includes the majority of tributaries upstream of the Molopo Canyon with two core areas located around the transition to the first escarpment as well as on top of the Kalahari Plateau (Fig. 6b). The third source area (cluster 3) consists mainly of eolian deposits situated on the Kalahari Plateau (Fig. 6c). Only few tributaries show a compositional signal similar to eolian deposits and are generally associated with dune complexes within their drainage areas as revealed by observations from satellite imagery.

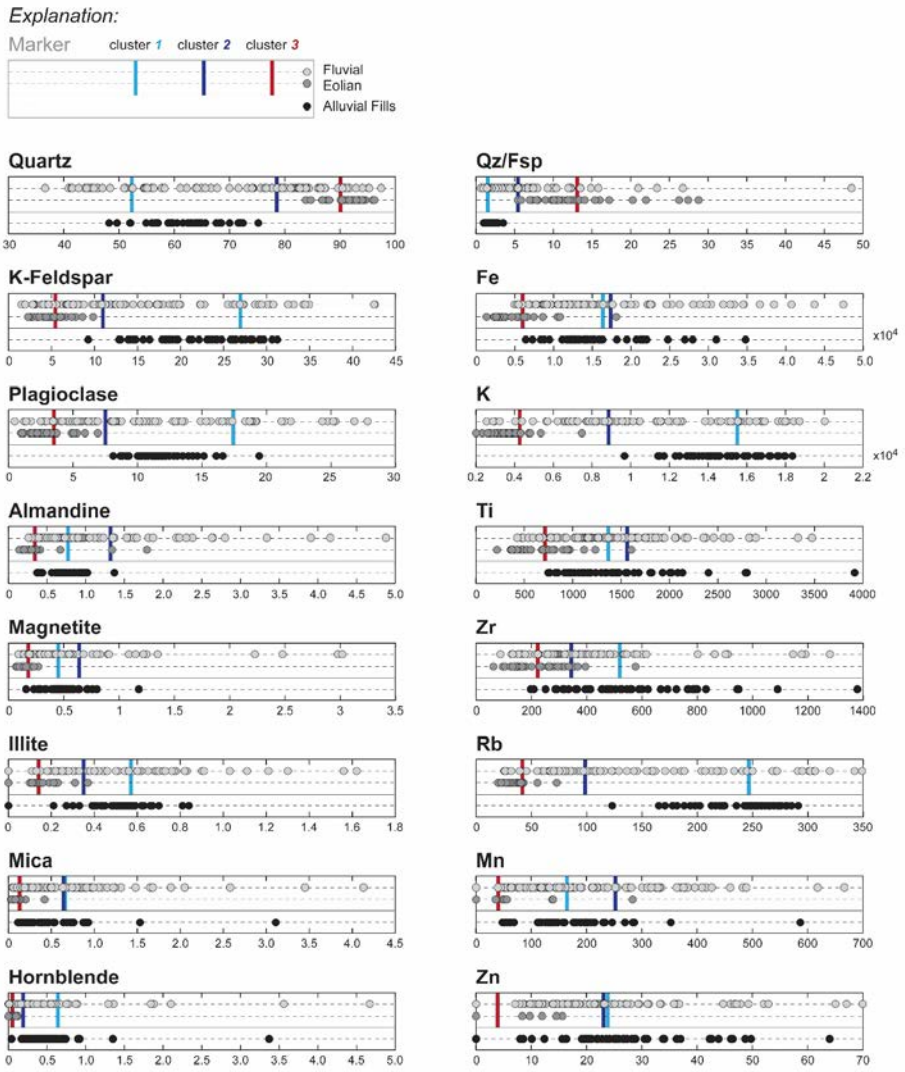

Fig. 5: Mineralogical and elemental cluster composition. Cluster center coordinates for cluster 1 to 3 are depicted as coloured vertical lines. Additionally, light grey to black dots indicate the composition of reference (OF and OA sample set) and profile samples. Units for minerals are given in percent, for elements in cps.

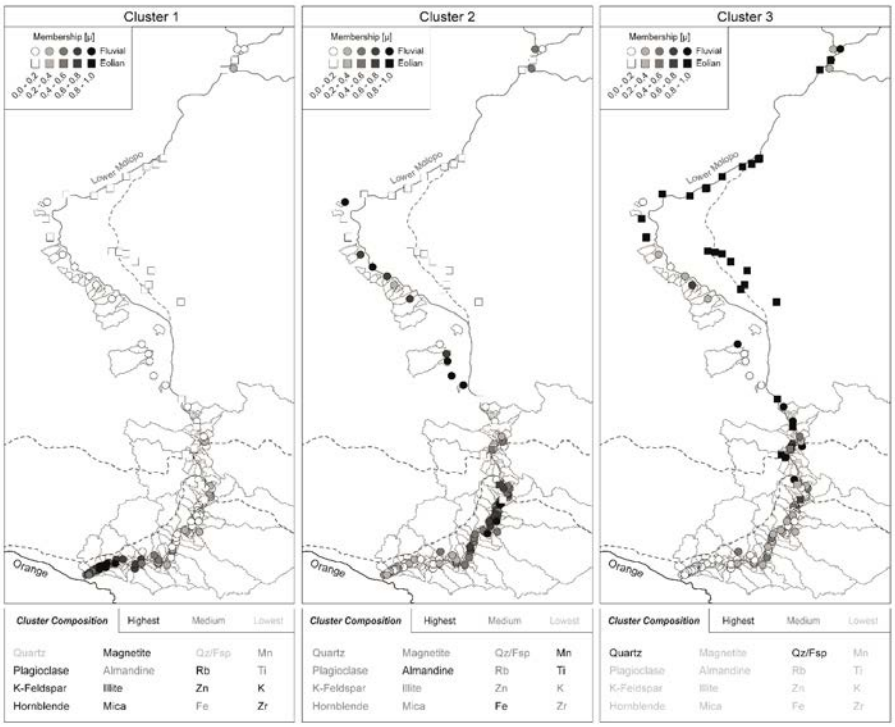

Fig. 6: Spatial distribution of membership degrees (μ) to mineralogical and elemental cluster center of reference samples. Light grey polygons delineate tributary catchments. Grey dashed lines delineate courses of the 1st and 2nd escarpment. Additionally, the mineralogical and elemental cluster composition as presented in Fig. 5 is illustrated at the bottom of each respective cluster.

To identify potential sediment provinces of fluvial deposits within the Molopo Canyon, we calculated the geochemical and mineralogical similarity (in μ) of the fine fraction (<2 mm) of bulk samples collected from key profiles to the previously calculated cluster center. The results of the fuzzy similarity analysis are presented in Fig. 7. Generally, fluvial deposits in the Molopo Canyon show highest similarities to cluster 1 with a mean μ of 0.64 to cluster 1 compared to a mean μ of 0.26 to cluster 2 and 0.10 to cluster 3. Hence, the results indicate local sediment sources for the origin of fluvial deposits within the canyon. However, this overall trend is temporally differentiated, with especially the oldest deposits of F_1 (profile 2820-107) showing the highest similarities to cluster 1 with a mean μ of 0.81 in a range of 0.92 to 0.67. Younger

444 deposits of level F_2 reveal variation in terms of µ. Especially fine grained layers (layer type 1)
445 show an increased µ to cluster 2 and hence indicate an increased contribution of distant fluvial
446 sediment sources, with a mean of 0.39 compared to a µ of 0.17 of the coarse grained layer type
447 2. Layer type 2, in turn, shows highest similarities to local sediment sources as expressed by a
448 mean µ of 0.74 to cluster 1. Highest similarities to distant fluvial sources occur in deposits of
449 level F_3 (profile 2820-136), in which five of the eleven analyzed layers reveal a dominant µ to
450 cluster 2 with a mean of 0.52. Similarities to eolian sources as expressed by µ to cluster 3 within
451 all studied profiles are low with a mean of 0.10 in a range of 0.03 to 0.28.

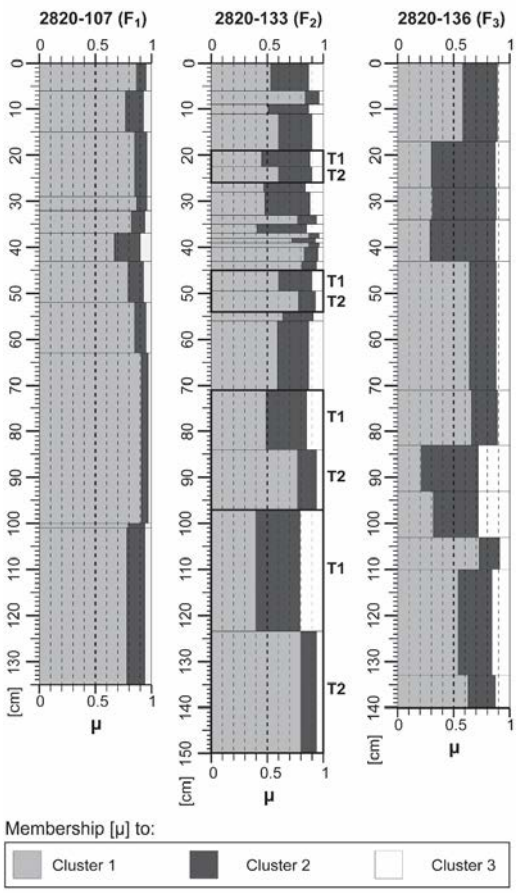

452

453 Fig. 7: **Mineralogical and elemental similarities of alluvial fills to reference cluster**. Similarities are expressed
454 by membership degrees (µ) of individual layers (as presented in Fig. 4) to cluster center 1 to 3. T1 and T2
455 correspond to mean values for layer type 1 and 2 respectively (see text).

5. Discussion

A luminescence chronology of fluvial deposits in the Molopo Canyon was established using quartz OSL dating. Overall, the quartz luminescence ages are considered to be reliable based on the agreement with feldspar ages or stratigraphic consistency. To gain insight into sediment dynamics during stages of valley aggradation, we applied a provenance analysis on the fine fraction of alluvial fill sediments. The provenance analysis was carried out by applying a FCM clustering routine to the mineralogical and elemental composition of the fine-fraction of potential sediment sources throughout the course of the lower Molopo (i.e., tributary sediments and eolian deposits). The analysis revealed three major potential sediment source areas: local sources from tributaries supplying the Molopo Canyon (cluster 1), regional sources from tributaries upstream of the Molopo Canyon (cluster 2) and far-distance sources from eolian deposits on the Kalahari plateau (cluster 3).

Sediments belonging to clusters 1 and 2 originate from tributary deposits along the course of the lower Molopo. The mineralogical composition dominated by quartz and feldspar in clusters 1 and 2 fits well to mineral assemblages reported for sediments derived from the Namaqua-Belt (Garzanti et al., 2014). Generally, the composition of clusters 1 and 2 reflects the widespread occurrence of metamorphic rock sources in the study area. In particular, the canyon area is dominated by the occurrence of the Riemvasmaak gneiss, a quartz-feldspar gneiss, likely accounting for the highest concentrations of plagioclase and K-feldspar and the associated concentration of potassium in cluster 1. Further, the subordinate occurrence of intrusive biotite-rich gneisses like the Donkieboud granite and Koelmanskop metamorphics explain the highest concentrations of minerals belonging to the mica group in cluster 1. Upstream of the canyon area, quartzites and gneiss belonging to the Korannaland and Nama Group dominate the geology near the 1st and 2nd escarpment, explaining an increase of quartz concentrations in cluster 2 compared to cluster 1. Additionally, subdominant occurrences of kinzigite and garnet-bearing granitic gneiss likely account for an increased concentration of almandine in cluster 2. We thus suggest that bedrock geology is the dominant forcing factor on the variability in the studied parameters.

Sediments belonging to cluster 3 are derived from eolian deposits throughout the Kalahari Plateau in the study area. The high content of quartz minerals in sediments of cluster 3 generally fit with a reported quartz content of >90% in Kalahari sands (Thomas and Shaw, 1991). Low elemental concentrations in Kalahari sediments are reported by Garzanti et al. (2014) in Middle Kalahari settings and are ascribed to extreme quartz dilution, thus accounting for low concentrations of elements in cluster 3. Since samples belonging to cluster 3 are derived from

superficial unconsolidated sediments, the temporal stability of the provenance signal for sediments of cluster 3 may be affected by Late Quaternary environmental change in the Kalahari interior. However, the Kalahari sand sheet is reported to be homogenous in terms of its mineralogical composition over large areas of the southwestern Kalahari (Thomas, 1987), thus minimizing the effect of potential Holocene sand dynamics on the mineralogical composition of cluster 3. Further, Hürkamp et al. (2011) and Heine (1990) inferred from linear dune formations on the Kalahari Plateau near the Molopo-Nossob confluence, that dune activity was highest during the Late Pleistocene with only subordinate activity phases during the Holocene.

We conclude that the signals provided by mineralogical and elemental concentrations are temporally stable indicators of provenance on Holocene time scales. However, due to the semi-quantitative nature of the applied methodology and uncertainties concerning the enrichment and depletion of single parameters, changes in the measured composition of alluvial fills do not reflect quantitative changes in sediment fluxes. Variations in membership degrees of fluvial sediments in the Molopo Canyon to sediment source areas are thus only probabilistic indicators of changes in sediment provenance.

5.1 Genetic interpretation of Holocene landscape development of the Molopo Canyon

The observed changes in the sedimentary archives of the Molopo Canyon suggest major changes in the fluvial system during the Holocene. There is no geomorphological evidence for a perennial flow regime of the lower Molopo within the reaches of the Molopo Canyon during the last ~9 ka, suggesting an ephemeral flow regime throughout the Holocene. On a conceptual level, it is well established that changes in the fluvial system of ephemeral river systems during flood events are caused by a balance between sediment supply and stream power (Harvey et al., 2011), a concept derived from the threshold of critical stream power (Bull, 1979). The balance of sediment supply and stream power is strongly influenced by local topography (Tooth, 2000), resulting in a spatial differentiation of deposition and erosion during flood events even within the same channel reach (Daniels, 2003). The spatial separation of fluvial processes is of special relevance for the Molopo Canyon environment, since a single rainfall event may cause spatially differentiated hydrological response in different reaches of the canyon: a highly energetic regime within bedrock tributaries caused by high gradients, an intermediate regime on transitional alluvial fans caused by moderate gradients, and a low energy regime within the flat valley floor. Based on quartz OSL dating of fluvial landforms encountered within the study

sections 1 to 3, we propose three major stages of Holocene fluvial activity in the Molopo Canyon. The temporal succession of stages covers the last ~9 ka of fluvial landscape development in the Molopo Canyon with only minor gaps in the fluvial record. Thus, quartz OSL dating of the identified fluvial landforms allows the first general classification of fluvial landscape development in the southwestern Kalahari during the Holocene. Further field investigations and analysis of previously unidentified fluvial archives might help to refine the proposed fluvial stratigraphy in this area.

Stage I – Valley aggradation

Stage I is characterized by an aggradation of the valley floor leading to the deposition of level F_1 between at least ~9 and ~6 ka. The deposits are characterized by a horizontal bedding of layers with varying degrees of sub-angular, matrix-supported gravel generally unsorted and without grading. Based on observations from the hyper-arid Arava Rift-valley in Israel, Laronne and Shlomi (2007) showed that horizontal bedding in single- or multi-thread gravel-bed streams is caused by single flood events, leading to the development of coarse grained event-strata in floodplain deposits. The ungraded character of such strata is interpreted as reflecting the flashiness of the flow regime, i.e., deposition in high magnitude events during short periods of time (Laronne and Shlomi, 2007). The deposition of F_1 as a consequence of flood induced vertical accretion of the floodplain is supported by the vertical age increment with depth as observed in profile 2820-106. The floodplain may represent the ephemeral counterpart to confined, coarse-textured floodplains as described by Nanson and Croke (1992) common for flood deposits in ephemeral streams (Daniels, 2003). In addition to the local origin of clasts as suggested by sub-angular clast shapes, the supporting matrix originates mainly from canyon tributaries as suggested by the highest similarities to cluster 1 of all studied fill deposits. Hence, we assume localized mobilization patterns in the deposition of alluvial fills during stage I. Thereby, the stream power generated during floods in this stage was high enough to cause erosion in steep tributary environments of the canyon and a subsequent transport through alluvial fans, but too low to cause further transport on the flat valley floor. We interpret the flood regime in this stage as a series of short-lived and localized flood events.

The almost complete removal of fill level F_1 indicates an episode of enhanced erosion in all parts of the Molopo Canyon following stage I. There is, however, no geomorphological or sedimentological evidence for sediment dynamics during the erosional stage as, for example, erosional landforms as observed in arroyo fill-cut sequences like scour-fill deposits (Mann and Meltzer, 2007). Despite the significance of this period for landscape development, implications on its nature and timing remain speculative based on the data presented here.

Stage II – Fan aggradation

Stage II is characterized by an aggradation of alluvial fans between ~6 and ~1.5 ka on a base level generated by the preceding phase of erosion within the canyon. The aggradation of alluvial fans buffered local sediment transport to the valley floor as evidenced by an absence of alluvial fill sediments within the Molopo Canyon during this stage. The absence of fills additionally indicates the absence of regional sediment supply from upstream of the Molopo Canyon during this stage. Uncertainties concerning this assumption remain, as an associated floodplain may be eroded or buried under younger floodplain deposits generated in the subsequent stage III. However, the aggradation of fans without a substantial deposition of valley fills as observed in the previous stage indicate lower rates of sediment mobilization, suggesting a decrease in the intensity of flood events during this stage.

Stage III – Valley aggradation

Phase III is characterized by a progressive aggradation of the valley floor between ~0.51 and 0.16 ka (not considering the age of sample KAL57). The aggradation led to the development of two fill levels: F_2 within deposits of a prograding alluvial fan in section 2 (Fig. 2) and F_3 associated with channel deposits within a confined valley environment unaffected by the local sedimentation of tributaries in section 3 (Fig. 2). Deposits of F_2 consist of couplets of horizontally bedded coarse and fine grained layers, a depositional form common for ephemeral streams in arid environments (Reid and Frostick, 2011). Frostick and Reid (1977) showed that the differentiation in grain sizes within these layer types results from a staggered sediment contribution from tributaries to the main flood wave and are thus a product of single flood events. The applicability of this concept to deposits of F_2 is reinforced by the contrasting provenance signal of coarse and fine grained layer couplets, which suggest a local origin of coarse grained layers corresponding to the contribution of local tributaries and an increased regional component in fine grained layers corresponding to the main flood wave (Fig. 4). Further, the prograding fan environment (Fig. 2) and a termination of fan aggradation prior to the deposition of F_2 suggest a recycling of fan material and the subsequent deposition in level F_2. The resulting short-distant transport paths of ~100 m may further explain the age inversion of the OSL ages observed in profile 2820-132 due to the insufficient or lack of bleaching of the sediment during transport for the layer in which sample KAL57 was collected. The increased similarities to regional sediment sources observed farther downstream in deposits of F_2 confirm the regional sediment contribution to flood events during this stage. We interpret the flood regime during this stage as a continuous series of large-scale flood events fed by the contribution of tributaries throughout the lower Molopo.

5.2 Paleoenvironmental interpretation

Paleoclimate is likely the dominant factor controlling Holocene fluvial activity in the Molopo Canyon. Human impact on the Holocene stream dynamics of the lower Molopo can be neglected, since an agricultural land-use in the form of extensive pastoralism started in the 19th century (Nash, 1996) towards the end of the Holocene record presented here. Additionally, tectonic activity is not ascribed to be a major cause for fluvial changes in the southern African interior during the late Pleistocene to Holocene (Dollar, 1998). Hence, we interpret the observed changes in flood regimes during stages I, II and III to indicate major shifts in the prevailing paleoclimatic conditions during the Holocene.

The early to mid-Holocene flash-flood regime in the lower Molopo of stage I coincides with a humid period on the African continent. The so-called 'African Humid Period' (AHP) is well documented throughout sedimentary archives in Africa and evidenced by the onset of wetter conditions during the early to mid-Holocene as recorded in ocean sediments (Adkins et al., 2006), lake sediments (Burrough and Thomas, 2008, Tierney and deMenocal, 2013), speleothem records (Burney et al., 1994) or *hyrax* middens (Chase et al., 2010). Although the AHP is believed to have had a spatially differentiated impact on environmental systems in the southern African interior (Burrough and Thomas, 2013), it is generally accepted that moisture availability increased in response to orbital forcing and shifts in the tropical circulation system (deMenocal et al., 2000, Tierney and deMenocal, 2013). Therefore, the early to mid-Holocene moisture optimum is evidenced predominantly in archives of the SRZ. It is thus likely, that flooding in the southwestern Kalahari during that episode is connected to an enhanced tropical easterly circulation and an associated increase in convective storm cells. Convective storm cells are known for their intense, short-lived character in the Kalahari during austral summer (Mphale et al., 2014). In addition to their short duration, convective storm cells are typically less than a few km in diameter (Reid and Frostick, 2011). An intense, short lived and spatially limited character of storms during the early Holocene would explain localized sediment mobilization patterns and the observed dispositional character of coarse grained event strata during valley aggradation. We thus assume a connection of valley aggradation in stage I to an early Holocene intensification of tropical easterly storm tracks.

Although the exact timing of the AHP termination is still debated, the quasi-synchronous valley-wide end of valley aggradation around ~6 ka predates the assumed termination of the AHP between 5.0 (Tierney and deMenocal, 2013) and 5.5 ka (Adkins et al., 2006). It is possible that the erosion of valley level F_1 occurred towards the end of the AHP. Subsequently, the

establishment of a low intensity flood regime in the Molopo Canyon as expressed by an aggradation of alluvial fans during stage II suggests decreased flood intensities between 6.1 and 1.5 ka. This stage coincides with an aridification trend evidenced in both the SRZ (Marchant and Hooghiemstra, 2004) and WRZ (Chase et al., 2010). The closest continuous archive to the lower Molopo also evidences drier conditions in the speleothem record of the Equus Cave around 4 ka (Johnson et al., 1997). We thus interpret the stage of fan aggregation as a stage of low intense rainfalls.

The second phase of valley aggradation during stage III in the interval of 0.51 ± 0.05 and 0.16 ± 0.02 ka falls into the global cooling phase of the Little Ice Age (LIA). Speleothem (Tyson et al., 2000) and ocean records (Farmer et al., 2005) from southern Africa indicate lower temperatures during this interval, probably in response to solar variability (Chambers et al., 2014). The cooling episode had a strong influence on the hydroclimatic regime of southern Africa, differentiated into drier conditions in the SRZ and YRZ (Bousmann and Scott, 1994; Wündsch et al., 2016) and wetter conditions in the WRZ (Hahn et al., 2015; Zhao et al., 2016). Based on paleoflood deposits in the Buffels River (South Africa), Benito et al. (2011) linked wetter conditions in the SRZ to an increase in the magnitude and frequency of flood events during the LIA in near coast environments of South Africa. The increase in flood intensity and frequency during the LIA is also evidenced by paleoflood deposits in dry valley systems throughout the Namib Desert (Heine, 2005, 2006; Heine and Völkel, 2011). Missionary correspondence of early European settlers document seasonal flooding events towards the end of the LIA in the Kalahari (Shaw et al., 1992; Nash and Endfield, 2002) also documented for the lower Molopo region (Nash, 1996). It is now widely believed that an increase in precipitation intensities during the LIA was caused by an equatorward migration of the westerly circulation, causing a northward shift of temperate frontal systems in austral winter (Lamy et al., 2001; Hahn et al., 2015). In contrast to the spatially limited character of convective storm cells in austral summer, Jury (2010) showed that, based on instrumental observations, flood-producing cloud bands over the Kalahari in austral winter can be several hundred kilometers in dimension. Intensification in the magnitude and/or frequency of supra-regional floods would explain the synchronous activation of tributaries during single flood events throughout the lower Molopo. Hence, we assume a predominant influence of the mid-latitude westerly circulation on the flood regime of the lower Molopo during the LIA.

Despite the regionality of seasonal flood events during the LIA, we did not detect an increase in sediment mobilization from eolian deposits originating from the Kalahari sand sheet north of the 2nd escarpment (cluster 3). This may be due to either (a) the applied methodology or (b)

658 a limited sediment outflow from the Kalahari to the lower Molopo. Methodological constraints
659 seem reasonable since the mineralogical and elemental composition of sediments belonging to
660 cluster 3 is characterized by low concentrations of all parameters with the exception of quartz
661 (Fig. 5). Hence, the elemental and mineralogical fingerprint of sediments consisting of eolian
662 sands from the Kalahari which are transported by a flood downstream would almost certainly
663 be altered to reflect the spectrum of active tributaries during the passage through the lower
664 Molopo. However, we would expect a detectable increase in the Qz/Fsp ratio by the transport
665 of quartz enriched Kalahari sediments. Since the Qz/Fsp ratio of all alluvial sediments in the
666 Molopo Canyon are in a range explained by bedrock composition of tributaries of the lower
667 Molopo (Fig. 5), we assume no relevant methodological constraint. Still, uncertainties
668 concerning this assumption remain and could be addressed by including an analysis of heavy
669 minerals known to occur in Kalahari sands (Thomas and Shaw, 1991). A limited sediment
670 supply from the Kalahari to the lower Molopo, in turn, is suggested by missionary
671 correspondence of the late 19th century (Nash, 1996) and anecdotal evidence from local farmers,
672 who report that the maximal south-extent of floods originating from the Kalahari during the last
673 century was near Abiquas Puts (see 4 in Fig. 1b). Heine (1981) reported dunes crossing the
674 Molopo valley south of Abiquas Puts, indicating the absence of fluvial discharge during the late
675 Holocene. A possible reason for the blockage is given by the physical properties of
676 unconsolidated sands, which are known to induce high rates of transmission losses during flood
677 events in ephemeral streams (Cataldo et al., 2010) due to high rates of channel bed infiltration
678 (Reid and Frostick, 2011). Transmission losses, dune complexes within the channel reaches and
679 high sediment concentrations in flood waters due to the availability of erodible sands would
680 progressively reduce the stream powers of flood waves originating from the Kalahari and lead
681 to deposition within upper reaches of the lower Molopo. If true, the missing sediment link
682 between the southwestern Kalahari and the Orange River bears important implications for
683 reconstructions of the terrestrial sediment supply from the southern African interior to the
684 Atlantic Ocean.

Commented [LS1]: Does not appear in reference list

6. Conclusion

Fluvial landforms in the Molopo Canyon provide a nearly continuous archive of fluvial dynamics during flood events in the southwestern Kalahari Desert for the last 8.8 ka. The hydrological regime of the lower Molopo remained ephemeral throughout the Holocene. Three major stages in flood dynamics during the Holocene are identified. The early Holocene was characterized by an aggradation of the canyon between ~9 to ~6 ka, leading to the deposition of alluvial fills. The aggradation was a consequence of intense, short-lived and spatially limited flood events which led to localized sediment mobilization patterns within the canyon. The occurrence of intense spatial and temporal storm cells is explained by a poleward shift of convective storm tracks associated with the tropical-easterly circulation. Since 6.1 ka, the aggradation of alluvial fans upstream of canyon tributaries without the deposition of alluvial fills evidences a decrease in runoff intensities probably related to a decrease in average storm intensity and/or frequency. The exact duration of fan aggradation is difficult to constrain due to the dissection and erosion of alluvial fans in the subsequent stage, but there is evidence for a duration of at least 4.6 ka until 1.5 ka ago. A second stage of valley aggradation occurred in the late Holocene from 0.51±0.05 to 0.16±0.02 ka, coinciding with the Little Ice Age. Alluvial fill deposits of this stage exhibit a characteristic sequence of event layers with each layer separated in a local and regional sediment component. The regional contribution of sediments upstream of the canyon during individual flood events is attributed to an intensification of supra-regional flood events associated with a poleward shift in frontal systems linked to the temperate westerly circulation. The nature and timing of the most significant episode of flooding within the Molopo Canyon, as evidenced by a complete removal of early Holocene valley fills, could not be dated in this study, but is constrained to occur sometime between 6.1±0.4 and 0.51±0.05 ka, possibly towards the end of the African Humid Period. Further, the Holocene sediment contribution from the lower Molopo to the perennial flow regime of the Orange River originated from the southernmost ~80 km of the lower Molopo without a detectable contribution from the Kalahari interior.

References

Adkins, J., deMenocal, P.B., Eshel, G., 2006. The “African humid period” and the record of marine upwelling from excess 230Th in Ocean Drilling Program Hole 658C. Paleoceanography 21(4), PA4203.

Bateman, M.D., Thomas, D.S., Singhvi, A.K., 2003. Extending the aridity record of the Southwest Kalahari: current problems and future perspectives. Quaternary International 111(1), 37-49.

Benito, G., Thorndycraft, V.R., Rico, M.T., Sánchez-Moya, Y., Sopeña, A., Botero, B.A., Machado, M.J., Davis, M., Pérez-González, A, 2011. Hydrological response of a dryland ephemeral river to southern African climatic variability during the last millennium. Quaternary Research 75(3), 471-482.

Bousman, B., Scott, L., 1994. Climate or overgrazing? The palynological evidence for vegetation change in the eastern Karoo. South African Journal of Science 90(11), 575-578.

Brook, G.A., Scott, L., Railsback, L.B., Goddard, E.A., 2010. A 35ka pollen and isotope record of environmental change along the southern margin of the Kalahari from a stalagmite and animal dung deposits in Wonderwerk Cave, South Africa. Journal of Arid Environments 74(7), 870-884.

Bull, W.B., 1979. Threshold of critical power in streams. Geological Society of America Bulletin 90(5), 453-464.

Burney, D.A., Brook, G.A., Cowart, J.B., 1994. A Holocene pollen record for the Kalahari Desert of Botswana from a U-series dated speleothem. The Holocene 4, 225–232.

Burrough, S.L., Thomas, D.S.G., 2008. Late Quaternary lake-level fluctuations in the Mababe Depression: Middle Kalahari palaeolakes and the role of Zambezi inflows. Quaternary Research 69(3), 388-403.

Burrough, S.L., Thomas, D.S.G., 2013. Central southern Africa at the time of the African Humid Period: a new analysis of Holocene palaeoenvironmental and palaeoclimate data. Quaternary Science Reviews 80, 29-46.

Bzedek, J., 1981. Pattern recognition with fuzzy objective function algorithms. Plenum Press, New York.

Cataldo, J.C., Behr, C., Montalto, F.A., Pierce, R.J., 2010. Prediction of transmission losses in ephemeral streams, Western USA. The Open Hydrology Journal 4(1), 19-34.

Chambers, F.M., Brain, S.A., Mauquoy, D., McCarroll, J., Daley, T., 2014. The ‘Little Ice Age’ in the Southern Hemisphere in the context of the last 3000 years: Peat-based proxy-climate data from Tierra del Fuego. The Holocene 24(12), 1649-1656.

Chase, B.M., Meadows, M.E., 2007. Late Quaternary dynamics of southern Africa's winter rainfall zone. Earth-Science Reviews 84(3), 103-138.

748 Chase, B.M., Meadows, M.E., Carr, A.S., Reimer, P.J., 2010. Evidence for progressive
749 Holocene aridification in southern Africa recorded in Namibian hyrax middens: implications
750 for African Monsoon dynamics and the ‘‘African Humid Period’’. Quaternary Research
751 74(1), 36-45.

752 Chase, B.M., Boom, A., Carr, A.S., Carré, M., Chevalier, M., Meadows, M.E., Pedro, J.B.,
753 Stager, J.C. Reimer, P.J., 2015a. Evolving southwest African response to abrupt deglacial
754 North Atlantic climate change events. Quaternary Science Reviews 121, 132-136.

755 Chase, B.M., Lim, S., Chevalier, M., Boom, A., Carr, A.S., Meadows, M.E., Reimer, P.J.
756 2015b. Influence of tropical easterlies in the southwestern Cape of Africa during the
757 Holocene. Quaternary Science Reviews 107, 138-148.

758 Chase, B.M., Meadows, M.E., Scott, L., Thomas, D.S.G., Marais, M., Sealy J., Reimer, P.J.,
759 2009. A record of rapid Holocene climate change preserved in hyrax middens from
760 southwestern Africa. Geology 37, 703–706.

761 Chase, B.M., Quick, L.J., Meadows, M.E., Scott, L., Thomas, D.S.G., Reimer, P.J., 2011.
762 Late glacial interhemispheric climate dynamics revealed in South African hyrax middens.
763 Geology 39, 19-22.

764 Chase, B.M., Scott, L., Meadows, M.E., Gil-Romera, G., Boom, A., Carr, A.S., Reimer, P.J.,
765 Truc, L., Valsecchi, V., Quick, L.J., 2012. Rock hyrax middens: A palaeoenvironmental
766 archive for southern African drylands. Quaternary Science Reviews 56, 107-125.

767 Christensen, J.H., Kumar, K.K., Aldrian, E., An, S.I., Cavalcanti, I.F.A, de Castro, M., Dong,
768 W., Goswami, P., Hall, A., Kanyanga, J.K., Kitoh, A., Kossin, J., Lau, N.C., Renwick, J.,
769 Stephenson, D.B., Xie, S.P., Zhou, T., 2013. Climate Phenomena and their Relevance for
770 Future Regional Climate Change. In: Stocker, T.F., Qin, D., Plattner, G.K., Tignor, M., Allen,
771 S.K., Boschung, J., Nauels, A., Xia, Y., Bex, V. and Midgley, P.M. (eds.), Climate Change
772 2013: The Physical Science Basis. Contribution of Working Group I to the Fifth Assessment
773 Report of the Intergovernmental Panel on Climate Change. Cambridge University Press,
774 Cambridge, UK and NY., pp. 1217-1308.

775 Cockcroft, M.J., Wilkinson, M.J., Tyson, P.D., 1987. The application of a present-day
776 climatic model to the late Quaternary in southern Africa. Climatic Change 10(2), 161-181.

777 Cunningham, A.C., Wallinga, J., 2010. Selection of integration time intervals for quartz OSL
778 decay curves. Quaternary Geochronology 5, 657-666.

779 Daniels, J.M., 2003. Floodplain aggradation and pedogenesis in a semiarid environment.
780 Geomorphology 56(3), 225-242.

781 deMenocal, P.B., Ortiz, J., Guilderson, T., Adkins, J., Sarnthein, M., Baker, L., Yarusinsky,
782 M., 2000. Abrupt onset and termination of the African Humid Period: rapid climate responses
783 to gradual insolation forcing. Quaternary Science Reviews 19(1), 347-361.

784 Dollar, E.S., 1998. Palaeofluvial geomorphology in southern Africa: a review. Progress in
785 Physical Geography 22(3), 325-349.

786 Dougill, A.J., Thomas, A.D., 2002. Nebkha dunes in the Molopo Basin, South Africa and
787 Botswana: formation controls and their validity as indicators of soil degradation. Journal of
788 Arid Environments 50(3), 413-428.

789 Dunn, J.C., 1973. A Fuzzy Relative of the ISODATA Process and Its Use in Detecting
790 Compact Well-Separated Clusters. Journal of Cybernetics 3(3), 32-57.

791 Farmer, E.C., deMenocal, P.B., Marchitto, T.M., 2005. Holocene and deglacial ocean
792 temperature variability in the Benguela upwelling region: Implications for low-latitude
793 atmospheric circulation. Paleoceanography 20(2), PA2018.

794 Frostick, L.E., Reid, I., 1977. The origin of horizontal laminae in ephemeral stream channel-
795 fill. Sedimentology 24(1), 1-9.

796 Garzanti, E., Andò, S., Vezzoli, G., 2009. Grain-size dependence of sediment composition
797 and environmental bias in provenance studies. Earth and Planetary Science Letters 277(3),
798 422-432.

799 Garzanti, E., Vermeesch, P., Padoan, M., Resentini, A., Vezzoli, G., Andò, S., 2014.
800 Provenance of passive-margin sand (southern Africa). The Journal of Geology 122(1), 17-42.

801 Guérin, G., Frouin, M., Talamo, S., Aldeias, V., Bruxelles, L., Chiotti, L., Dibble, H.L.,
802 Goldberg, P., Hublin, J.J., Jain, M., Lahaye, C., Madelaine, S., Maureille, B., McPherron,
803 S.P., Mercier, N., Murray, A.S., Sandgathe, D., Steele, T.E., Thomsen, K.J., Turq, A., 2015.
804 A multi-method luminescence dating of the Palaeolithic sequence of La Ferrassie based on
805 new excavations adjacent to the La Ferrassie 1 and 2 Skeletons. Journal of Archaeological
806 Science 58, 147-166.

807 Guérin, G., Mercier, N., Adamiec, C., 2011. Dose-rate conversion factors: update. Ancient TL
808 29, 5–8.

809 Hahn, A., Compton, J.S., Meyer-Jacob, C., Kirsten, K.L., Lucasssen, F., Mayo, M. Schefuß,
810 E., Zabel, M., 2015. Holocene paleo-climatic record from the South African Namaqualand
811 mudbelt: A source to sink approach. Quaternary International 404, 121-135.

812 Harvey, J.E., Pederson, J.L., Rittenour, T.M., 2011. Exploring relations between arroyo cycles
813 and canyon paleoflood records in Buckskin Wash, Utah: Reconciling scientific paradigms.
814 Geological Society of America Bulletin 123(11-12), 2266-2276.

815 Heine, K.,1981. Aride und pluviale Bedingungen während der letzten Kaltzeit in der Südwest-
816 Kalahari (südliches Afrika). Ein Beitrag zur klimagenetischen Geomorphologie der Dünen,
817 Pfannen und Täler. Zeitschrift für Geomorphologie Supplement 38, 1-37.

818 Heine, K., 1990. Some observations concerning the age of the dunes in the western Kalahari
819 and palaeoclimatic implications. Palaeoecology of Africa and the surrounding islands 21, 161-
820 178.

821 Heine, K., 2005. Holocene climate of Namibia: a review based on geoarchives. African study
822 monographs 30, 119-133.

823 Heine, K., 2006. Slackwater deposits and floodouts as evidence for flash floods in Namib
824 Desert valleys, Namibia, and implications for settlements. In: Leser, H., (ed.), The changing
825 culture and nature of Namibia: case studies: the Sixth Namibia Workshop Basel 2005; in
826 honour of Carl Schlettwein (1925 - 2005). Basler Afrika-Bibliographien, Basel, pp. 159-163.

827 Heine, K., Völkel, J., 2011. Extreme floods around AD 1700 in the northern Namib Desert,
828 Namibia, and in the Orange River catchment, South Africa-Were they forced by a decrease of
829 solar irradiance during the Little Ice Age? Geographia Polonica 84, Special Issue Part 1, 61-
830 80.

831 Huntley, D.J., Baril, M.R., 1997. The K content of the K-feldspars being measured in optical
832 dating or in thermoluminescence dating. Ancient TL 15, 11-13.

833 Hürkamp, K., Völkel, J., Heine, K., Bens, O., Leopold, M., Winkelbauer, J., 2011. Late
834 Quaternary environmental changes from aeolian and fluvial geoarchives in the southwestern
835 Kalahari, South Africa: implications for past African climate dynamics. South African Journal
836 of Geology 114(3-4), 459-474.

837 Johnson, B.J., Miller, G.H., Fogel, M.L., Beaumont, P.B., 1997. The determination of late
838 Quaternary paleoenvironments at Equus Cave, South Africa, using stable isotopes and amino
839 acid racemization in ostrich eggshell. Palaeogeography, Palaeoclimatology, Palaeoecology
840 136(1), 121-137.

841 Jury, M.R., 2010. Flood-producing cloud bands over the Kalahari Desert. Theoretical and
842 applied climatology 102(3-4), 367-378.

843 Lamy, F., Hebbeln, D., Röhl, U., Wefer, G., 2001. Holocene rainfall variability in southern
844 Chile: a marine record of latitudinal shifts of the Southern Westerlies. Earth and Planetary
845 Science Letters 185(3), 369-382.

846 Laronne, J.B., Shlomi, Y., 2007. Depositional character and preservation potential of coarse-
847 grained sediments deposited by flood events in hyper-arid braided channels in the Rift Valley,
848 Arava, Israel. Sedimentary Geology 195(1), 21-37.

849 Long, H., Shen, J., Wang, Y., Gao, L., Frechen, M., 2015. High-resolution OSL dating of a
850 late Quaternary sequence from Xingkai Lake (NE Asia): Chronological challenge of the "MIS
851 3a Mega-paleolake" hypothesis in China. Earth and Planetary Science Letters 428, 281-292.

852 Madsen, A.T., Buylaert, J.P., Murray, A.S., 2011. Luminescence dating of young coastal
853 deposits from New Zealand using feldspar. Geochronometria 38, 378-390.

854 Mann, D.H., Meltzer, D.J., 2007. Millennial-scale dynamics of valley fills over the past
855 12,000 14C yr in northeastern New Mexico, USA. Geological Society of America Bulletin
856 119(11-12), 1433-1448.

857 Marchant, R., Hooghiemstra, H., 2004. Rapid environmental change in African and South
858 American tropics around 4000 years before present: a review. Earth-Science Reviews 66(3),
859 217-260.

860 Milligan, G.W., Cooper, M.C., 1988. A study of standardization of variables in cluster
861 analysis. Journal of classification 5(2), 181-204.

862 Mphale, K.M., Dash, S.K., Adedoyin, A., Panda, S.K., 2014. Rainfall regime changes and
863 trends in Botswana Kalahari Transect's late summer precipitation. Theoretical and applied
864 climatology 116(1-2), 75-91.

865 Murray, A.S., Wintle, A.G., 2003. The single aliquot regenerativedose protocol: potential for
866 improvements in reliability. Radiation Measurement 37, 377–381.

867 Murray, A.S., Wintle, A.G., 2000. Luminescence dating of quartz using an improved single-
868 aliquot regenerative-dose protocol. Radiation measurements 32(1), 57-73.

869 Murray, A.S., Marten, R., Johnston, A., Martin, P., 1987. Analysis for naturally occurring
870 radionuclides at environmental concentrations by gamma spectrometry. Journal of
871 Radioanalytical and Nuclear Chemistry 115, 263–288.

872 Murray, A.S., Thomsen, K.J., Masuda, N., Buylaert, J.P., Jain, M., 2012. Identifying well-
873 bleached quartz using the different bleaching rates of quartz and feldspar luminescence
874 signals. Radiation Measurements 47, 688–695.

875 Nanson, G.C., Croke, J.C., 1992. A genetic classification of floodplains. Geomorphology
876 4(6), 459-486.

877 Nash, D.J., 1996. On the dry valleys of the Kalahari: documentary evidence of environmental
878 change in central southern Africa. Geographical Journal 162(2), 154-168.

879 Nash, D.J., Endfield, G.H., 2002. Historical flows in the dry valleys of the Kalahari identified
880 from missionary correspondence. South African journal of science 98(5-6), 244-248.

881 Opitz, S., Ramisch, A., IJmker, J., Lehmkuhl, F., Mischke, S., Stauch, G., Wünnemann, B.,
882 Zhang, Y., Diekmann, B., 2016. Spatio-temporal pattern of detrital clay-mineral supply to a
883 lake system on the north-eastern Tibetan Plateau, and its relationship to late Quaternary
884 paleoenvironmental changes. Catena 137, 203-218.

885 Peeters, J., Busschers, F.S., Stouthamer, E., Bosch, J.H.A., Van den Berg, M.W., Wallinga, J.,
886 Versendaal, A.J., Bunnik, F.P.M., Middelkoop, H., 2016. Sedimentary architecture and
887 chronostratigraphy of a late Quaternary incised-valley fill: A case study of the late Middle and
888 Late Pleistocene Rhine system in the Netherlands. Quaternary Science Reviews 131, 211-236.

889 Prescott, J.R., Hutton, J.T., 1994. Cosmic ray contributions to dose rates for luminescence and
890 ESR dating: large depths and long-term time variations. Radiation Measurements 23, 497-
891 500.

892 Raab, T., Hürkamp, K., Völkel, J., 2005. Detection and Quantification of Heavy Metal
893 Contamination in Alluvial Soils of Historic Mining Areas by Field Portable X-ray Fluorescence
894 (FPXRF) Analysis. Proceedings of International Conference On Problematic Soils, Eastern
895 Mediterranean University, Famagusta, pp. 299-306.

896 Ramisch, A., Lockot, G., Haberzettl, T., Hartmann, K., Kuhn, G., Lehmkuhl, F., Schimpf, S.,
897 Schulte, P., Stauch, G., Wang, R., Wünnemann, B., Yan, D., Zhang, Y., Diekmann, B., 2016.
898 A persistent northern boundary of Indian Summer Monsoon precipitation over Central Asia
899 during the Holocene. Scientific Reports 6, 25791.

900 Reid, I., Frostick, L.E., 2011. Channel form, flows and sediments of endogenous ephemeral
901 rivers in deserts. In: Thomas, D.S.G. (ed.), Arid Zone Geomorphology: Process, Form and
902 Change in Drylands. John Wiley & Sons Ltd, Chichester, UK, pp. 301-332.

903 Reimann, T., Notenboom, P.D., De Schipper, M.A., Wallinga, J., 2015. Testing for sufficient
904 signal resetting during sediment transport using a polymineral multiple-signal luminescence
905 approach. Quaternary Geochronology 25, 26-36.

906 Rémillard, A.M., St-Onge, G., Bernatchez, P., Hétu, B., Buylaert, J.P., Murray, A.S.,
907 Vigneault, B., 2016. Chronology and stratigraphy of the Magdalen Islands archipelago from
908 the last glaciation to the early Holocene: new insights into the glacial and sea-level history of
909 eastern Canada. Boreas 45, 604-628.

910 Rittenour, T.M., 2008. Luminescence dating of fluvial deposits: applications to geomorphic,
911 paleoseismic and archaeological research. Boreas 37, 613–635.

912 Shaw, P.A., Thomas, D.S., Nash, D.J., 1992. Late Quaternary fluvial activity in the dry
913 valleys (mekgacha) of the Middle and Southern Kalahari, southern Africa. Journal of
914 Quaternary Science 7(4), 273-281.

915 Stone, A.E.C., Thomas, D.S.G., 2008. Linear dune accumulation chronologies from the
916 southwest Kalahari, Namibia: challenges of reconstructing late Quaternary
917 palaeoenvironments from aeolian landforms. Quaternary Science Reviews 27(17), 1667-1681.

918 Sugisaki, S., Buylaert, J.P., Murray, A.S., Tada, R., Hongbo, Z., Ke, W. Saito, K., Chao, L.,
919 Li, S., Irino, T., 2015. OSL dating of fine-grained quartz from Holocene Yangtze delta
920 sediments. Quaternary Geochronology 30, 226-232.

921 Thomas, D.S.G., 1987. Discrimination of depositional environments using sedimentary
922 characteristics in the Mega Kalahari, central southern Africa. In: Frostick, L., Reid, I. (eds.),
923 Desert Sediments: Ancient and Modern, Geological Society, London, Special Publications
924 35(1), pp. 293-306.

925 Thomas, D.S.G., Shaw, P.A., 1991. The Kalahari environment. Cambridge University Press,
926 Cambridge.

927 Thomas, D.S., O'Connor, P.W., Bateman, M.D., Shaw, P.A., Stokes, S., Nash, D.J., 2000.
928 Dune activity as a record of late Quaternary aridity in the Northern Kalahari: new evidence

from northern Namibia interpreted in the context of regional arid and humid chronologies. Palaeogeography, Palaeoclimatology, Palaeoecology 156(3), 243-259.

Thomsen, K.J., Bøtter-Jensen, L., Denby, P.M., Moska, P., Murray, A.S., 2006. Developments in luminescence measurement techniques. Radiation Measurements 41, 768-773.

Tierney, J.E., deMenocal, P.B., 2013. Abrupt shifts in Horn of Africa hydroclimate since the Last Glacial Maximum. Science 342(6160), 843-846.

Tooth, S., 2000. Process, form and change in dryland rivers: a review of recent research. Earth-Science Reviews 51(1), 67-107.

Tyson, P.D., 1986. Climatic Change and Variability in Southern Africa. Oxford University Press, Cape Town.

Tyson, P.D., Karlen, W., Holmgren, K., Heiss, G.A., 2000. The little ice age and Medieval warming in South Africa. South African Journal of Science 96(3), 121-126.

Wu, K.L., Yang, M.S., 2005. A cluster validity index for fuzzy clustering. Pattern Recognition Letters 26(9), 1275-1291.

Wündsch, M., Haberzettl, T., Kirsten, K.L., Kasper, T., Zabel, M., Dietze, E., Baade, J., Daut, G., Meschner, S., Meadows, M.E., Mäusbacher, R., 2016. Sea level and climate change at the southern cape coast, South Africa, during the past 4.2 kyr. Palaeogeography, Palaeoclimatology, Palaeoecology 446, 295-307.

Xie, X.L., Beni, G., 1991. A validity measure for fuzzy clustering. IEEE Transactions on Pattern Analysis & Machine Intelligence 8, 841-847.

Zhao, X., Dupont, L., Schefuß, E., Meadows, M.E., Hahn, A., Wefer, G., 2016. Holocene vegetation and climate variability in the winter and summer rainfall zones of South Africa. The Holocene 26(6), 1-15.

Acknowledgements

This study was funded by the German Federal Ministry of Education and Research (BMBF) as part of the joint project “GeoArchives – Signals of Climate and Landscape Change preserved in Southern African GeoArchives” (No. 03G0838A) within the “SPACES Program – Science Partnerships for the Assessment of Complex Earth System Processes“ research initiative. We are greatly thankful for the access to private farmland provided by local farmers throughout the course of the lower Molopo during the field campaign in 2015. Additionally we wish to thank Jörg Erzinger and Anna Maria Schleicher for providing the quantitative XRF measurements conducted at the GFZ Potsdam. Jan-Pieter Buylaert receives funding from the European Research Council (ERC) under the European Union’s Horizon 2020 research and innovation programme ERC-2014-StG 639904 – RELOS. Vicki Hansen and Louise M. Helsted are thanked for their help with sample preparation for luminescence dating analyses.